Chapter 1

Introduction

The introductory chapter is devoted to the nature of combustion-generated nanoparticles, with a particular focus on soot and silica. The concept of fractal aggregate particles is introduced, and simple theoretical model describing their growth is discussed. Finally, an overview of this thesis is given.

1.1. Combustion-generated particles

Combustion is the main source of power and heat. However, the process of combustion also results in the production of various pollutants. While the focus nowadays is often on greenhouse gases, combustion-generated particles such as soot have an impact not only on the environment, but also on combustion equipment and human health [1–6]. This impact is strongly linked to the particles' size and structure, which are both dependent on the conditions in which the particles are formed. Probably of most interest are particles in the nanometer size range. The term nanoparticle is generally used to refer to particles with diameter around 100 nm or smaller. Particles in this class typically behave differently from bulk material.

Broadly speaking, some species formed in combustion will condense into small clusters, which in turn collide with other molecules and clusters. In latter stages, small spherical clusters, commonly referred to as primary particles or monomers, form the basis of what are known as fractal aggregates.

1.2. Fractal aggregates

Structures such as the ones formed in combustion, which are the result of particles getting lumped together into clusters, all form in a similar manner. Atoms or molecules M condense into small clusters, which in turn collide with other molecules and clusters, forming larger structures. For two particles, containing i and j molecules respectively, association can be schematically represented as:

$$M_i + M_j \rightarrow M_{i+j} \,. \tag{1.1}$$

At the initial stages of cluster growth, complete coagulation of colliding particles is near-instantaneous, meaning that clusters tend to be spherical as a result of minimizing surface energy. However, as the clusters grow—especially accompanied by a drop in temperature further from the flame front—complete coalescence or sintering of the clusters may become slow compared to the time between collisions. In this scenario particles may still merge somewhat, so that necks are formed at the contact points, but the individual building blocks (called monomers or primary particles) of the cluster remain recognizable. Association of larger numbers of particles in this way results in dendrite-shaped structures like those shown later in this chapter, in Figure 1.5, called fractal aggregates.

In the latter stages of growth particles may get joined loosely together without actually fusing, getting entangled into structures, 'agglomerates', that (compared to aggregates) can easily be broken by mechanical force. We note here that the terms aggregate and agglomerate are used interchangeably by many, an issue that has been discussed in depth in [7] where it is proposed to instead use the terms 'soft agglomerate' for the loosely joined particles, and 'hard agglomerate' for the fused structures. In the remainder of this work we will nevertheless stick to the terms aggregation and agglomeration as defined here in order to be consistent with similar work.

1.2.1. Aggregate structure

A convenient and oft-used measure of aggregate size is its mass-averaged root-mean-square radius a.k.a. radius of gyration R_g,

$$R_g = \sqrt{\frac{\sum m_i r_i^2}{\sum m_i}}, \tag{1.2}$$

with m_i the masses of the individual constituent particles of the aggregate, and r_i their position with respect to the aggregate's center of mass. In reality, aggregates will usually consist of particles of different sizes that have coalesced to varying degrees, and complex models may be constructed to take this into account. Still, it can be useful to use a slightly simplified representation, such as in Figure 1.1, where we assume a monodisperse

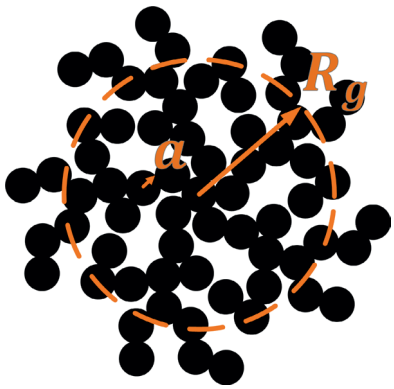

Figure 1.1. *Schematic 2-D representation of a fractal aggregate consisting of monomers with radius a. R_g denotes the aggregate's mass-averaged root-mean-square radius a.k.a. radius of gyration, defined in Eq. (1.2).*

monomer size distribution and limited coalescence so that the monomers constituting the aggregate can be considered spheres with radius a. Making these assumptions, R_g is related to the number of monomers inside an aggregate n as [8]

$$n = k_0 \left(\frac{R_g}{a}\right)^{D_f}, \tag{1.3}$$

where k_0 is a proportionality constant of order unity, and $D_f \leq 3$ is the fractal dimension. This means that the fractal aggregates can be defined by just three parameters: R_g, a, and D_f.

While more precise definitions of the fractal dimension exist, for our purposes it is sufficient to understand it as a measure for the way the amount of material scales with the objects outer dimensions, with high values corresponding to dense structures and low numbers with relatively porous structures. For clarity, this concept is illustrated in Figure 1.2 for structures in 2-D space. When the outer dimensions of the first structure scale with factor 3, its surface area scales with factor 8 (compared to factor 9 for a normal two-dimensional structure), giving a fractal dimension $D_f = 1.89$, and with factor 5 for the second structure, giving a much lower value of $D_f = 0.48$. As illustrated in Figure 1.3, the principle is exactly the same in 3-D space; when the outer dimensions of these structures scale with factor 3, the volumes of the first scales with factor 20 and the second with factor 9

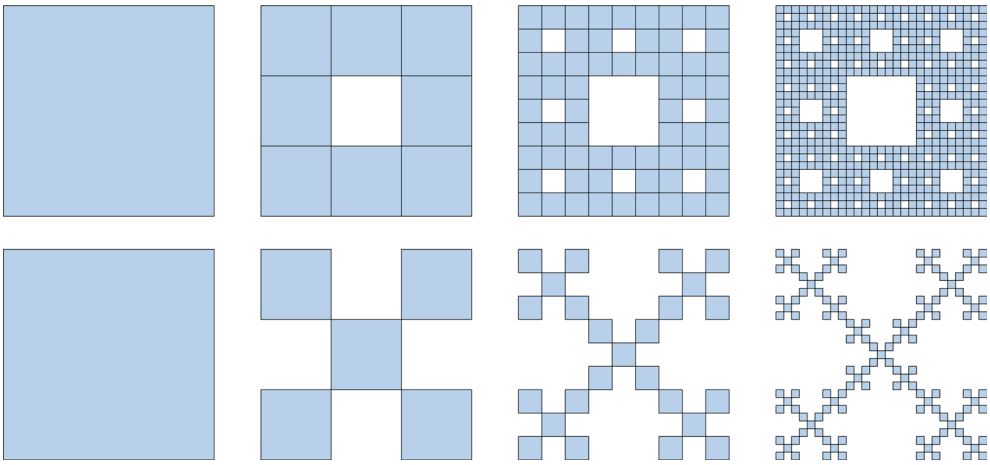

Figure 1.2. *Illustration of fractal dimension in 2-D space; when the outer dimensions scale with factor 3, the surface area scales with factor 8, giving a fractal dimension $D_f = 1.89$ (top), and with factor 5, giving a fractal dimension $D_f = 0.48$ (bottom).*

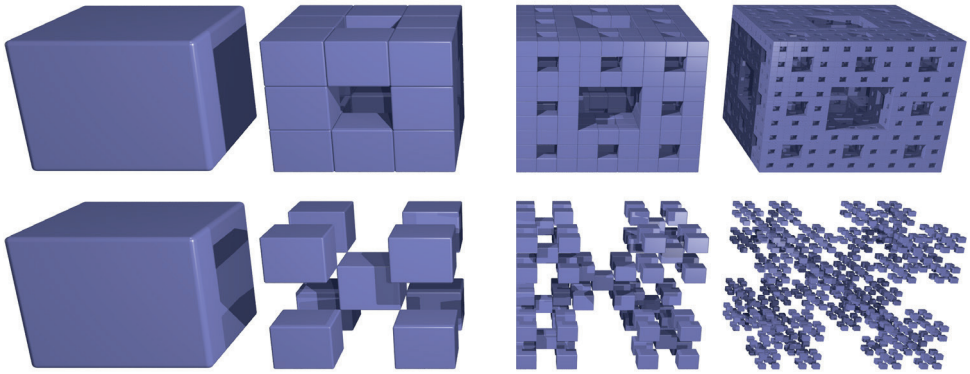

Figure 1.3. *Illustration of fractal dimension of similar objects in 3-D space; when the outer dimensions scale with factor 3, the volume scales with factor 20, giving a fractal dimension $D_f = 2.73$ (top), and with factor 9, giving a fractal dimension $D_f = 2$ (bottom).*

(compared to 27 for a normal three-dimensional structure), corresponding to fractal dimensions of 2.73 and 2, respectively.

Due to their fractal-like nature, the density of these particles decreases with aggregate size, resulting in a high surface to volume ratio. Furthermore, this type of structure significantly increases the collision frequency, and therefore the rate of particle growth, compared to solid spherical clusters of equal mass.

1.2.2. Time dependence of aggregate radius

To describe collisions between fractal aggregates, it is convenient to treat them as spherical particles having an effective collision radius r_c, which (owing to a relation akin to Eq. (1.3)) is related to the particle's volume v and surface area s as [9]

$$r_c = \frac{3v}{s}\left(\frac{s^3}{36\pi v^2}\right)^{1/D_f}, \tag{1.4}$$

with the fractal dimension, $D_f \leq 3$, depending on the mechanism of formation [10]. When $D_f = 3$, the collision radius is simply the particle's radius. But for the typical fractal dimensions of real fractal aggregates the collision radius is considerably larger than that of a spherical particle of equal mass. In the simple model where the fractal aggregate is presented as a set of spheres with radius a (as in Eq. (1.3)), its collision radius is to a good approximation equal to R_g.

Association according to Eq. (1.1) occurs with a corresponding rate of $R_{i,j}$, which represents the number of collisions per unit time per unit volume. This rate is given by $R_{i,j} = \epsilon_{i,j}\beta_{i,j}N_iN_j$ where N_i and N_j are the concentration of particles containing i and j molecules, respectively, $\epsilon_{i,j}$ is the sticking coefficient, and $\beta_{i,j}$ is the so-called collision kernel, which depends on both particle parameters and gas properties [11]. Of particular importance for determining $\beta_{i,j}$ is the ratio of the mean free path of the gas molecules λ and particle collision radius (given by Eq. (1.4)), defined as the Knudsen number $Kn = \lambda/r_c$ [9]. When the particle's radius is much larger than the mean free path ($Kn \ll 1$), molecules striking its surface are strongly affected by those leaving, so the attachment process is restricted by the diffusional approach of atoms in the buffer gas to the cluster. Conversely, when the particle's radius is much smaller than the mean free path ($Kn \gg 1$), molecules bouncing from its surface are unlikely to affect approaching molecules. In this case, which is representative for especially early stages of growth, attachment of new molecules is the result of pairwise collisions.

Both for $Kn \ll 1$ and $Kn \gg 1$ (continuum and free molecular regime respectively) theoretical expressions for the collision kernel are easily obtained [11]. For spherical particles in the free molecular regime $\beta_{i,j}$ is given by [11].

$$\beta_{i,j} = \left(\frac{3}{4\pi}\right)^{1/6}\left(\frac{6kT}{\rho_M}\right)^{1/2}\left(\frac{1}{v_i}+\frac{1}{v_j}\right)^{1/2}\left({v_i}^{1/3}+{v_j}^{1/3}\right)^2, \tag{1.5}$$

where ρ_M is the density of species M, and k is the Boltzmann constant. For two identical particles, the collision kernel is can thus be written as:

$$\beta = 4r_c^2\left(\frac{\pi kT}{\rho_M v}\right)^{1/2}. \tag{1.6}$$

When the particles grow bigger, we need to take into account the transition from the free molecular to continuum regime. This can be done using the semi-empirical Fuchs interpolation expression for the collision kernel [12,13] in which we replace the solid sphere radius by r_c:

$$\beta = 8\pi D r_c\left(\frac{r_c}{2r_c+\sqrt{2}g}+\frac{\sqrt{2}D}{cr_c}\right)^{-1}, \tag{1.7}$$

where D is the particle diffusion coefficient, c is the mean particle velocity, and g is a transition parameter [9].

Now, the time evolution of the number density of particles as they coagulate is described by the so-called Smoluchowski system of differential equations [10,14]:

$$\frac{df(v_{i+j})}{dt} = -f(v_{i+j})\int_0^\infty \epsilon_{i+j,j}\beta_{i+j,j}f(v_j)dv_i + \frac{1}{2}\int_0^\infty \epsilon_{i,j}\beta_{i,j}f(v_i)f(v_j)dv_j\,, \quad (1.8)$$

where $f(v)$ is the cluster size distribution function. Generally, this system cannot be solved analytically and it is necessary to use numerical methods. But, with a couple of assumptions, we can make a rough estimate of the rate of aggregate growth. In this analysis we will ignore chemistry, assuming that all of species M is present right from the start. This is a reasonable approximation for silica, for example, since oxidation of the silica precursors used in this thesis (siloxanes) is very fast. Furthermore we will assume a monodisperse particle distribution, so that the number density of particles N_p is given by:

$$N_p = \frac{N_{cp}\chi_M m_M}{\rho_M v}\,, \quad (1.9)$$

where N_{cp} is the number density of the combustion products, χ_M is the M mole fraction in the combustion products, and m_M is the molecular mass of M. Proceeding further with the analysis, we find the time dependence for the collision radius assuming that all of species M is bound in particles and the particle density of combustion products is constant. In this case, taking the sticking coefficient to be unity, the decay in aggregate number density N_p due to coagulation is given by [11]:

$$\frac{dN_p}{dt} = -\frac{1}{2}\bar{\beta}N_p^2\,, \quad (1.10)$$

where $\bar{\beta}$ is the particle size averaged collision kernel. Assuming that monomer radius $a = 3v/s$ is constant in time, and using the assumption of a monodisperse particle size distribution and $Kn \gg 1$, we can rewrite Eq. (1.6) as:

$$\beta = 4\left(\frac{3}{4\pi}\right)^{\frac{2}{D_f}}\left(\frac{\pi kT}{\rho_M}\right)^{\frac{1}{2}} a^{2-\frac{6}{D_f}} v^{\frac{2}{D_f}-\frac{1}{2}}\,. \quad (1.11)$$

Substituting Eqs. (1.9) and (1.11) into Eq. (1.10) and using relation (1.3) yields:

$$r_c \propto t^{2/(3D_f-4)}\,, \quad (1.12)$$

which gives a $t^{1.43}$ dependence for the typical fractal dimension of D_f ~1.8, much weaker than the dependence for solid spherical clusters, where $r_c \propto t^{2/5}$.

It is important to keep in mind that in actuality the story will be more complex. For one, a transition from the free-molecular to continuum regime will affect the rate of collisions. But also, internal changes in aggregates affect particle growth. Even at temperatures below the material's melting point particles do not just stick together, but as is well known [15], the growth process is actually a combination of particle collisions and simultaneous intra-aggregate fusion. Driven by a tendency to minimize surface energy, contacting monomers inside aggregates will tend to coalesce together into larger spheres, decreasing the total surface area with the rate:

$$\left(\frac{ds}{dt}\right)_{\text{sintering}} = -\frac{1}{\tau_s}\left(s - s_{\text{sph}}\right), \tag{1.13}$$

where a is the aggregate's surface area, and τ_s is the characteristic time to reduce s to the area s_{sph} of a solid sphere of equal mass [11]. If the sintering rate is fast compared to the collision rate we expect compact sphere-like particles to be formed, while relatively slow sintering will result in aggregate type particles. The sintering rate is a material specific property that is strongly dependent on the temperature and on the sintering mechanism.

1.3. Particle species

Many different particle species can be generated in combustion, but below we will focus on two: soot and silica.

1.3.1. Soot

Soot is the most prominent species of combustion-generated particle, consisting of carbonaceous agglomerates containing large numbers of carbon atoms. In fact, carbonaceous matter (mainly originating from the incomplete combustion of fossil fuels) is one of the primary components of anthropogenic fine particular matter in the Netherlands, which in turn makes up about three quarters of the total fine particulate matter [16]. Furthermore, incandescence of heated soot particles is responsible for the familiar yellow/orange luminescence that many flames have (e.g. the flame of a candle, Bunsen flames with low aeration). It is interesting to note that in some cases the formation of soot is

actually desired. For example, in industrial furnaces and heat generators its presence can serve to enhance heat transfer by radiation [17]. In most cases, however, inception and growth of soot are undesirable because of its deleterious effects, like its contribution to global warming [1,2] and carcinogenic effects [6,18].

Formation of soot during combustion occurs under conditions where there is limited oxygen available (note that soot is itself combustible). When enough oxygen is available, the overall combustion of hydrocarbons is described by:

$$C_xH_n + \left(x + \frac{n}{4}\right) O_2 \rightarrow xCO_2 + \frac{n}{2} H_2O \,, \tag{1.14}$$

and no soot will be formed. However, if there is insufficient oxygen to convert all fuel according to this equation, combustion will be incomplete. In this case other products are formed in addition to carbon dioxide and water, such as carbon monoxide, hydrogen, other hydrocarbons, and soot. Formation of soot, especially, is a highly complex process, that consists of a number of stages, as illustrated in Figure 1.4. During oxidation, the hydrocarbon fuel is degraded into small hydrocarbon radicals. Under fuel-rich conditions, these radicals form small hydrocarbons, in particular acetylene, C_2H_2. Addition of more radicals results in growing unsaturated (radical) hydrocarbons, which eventually form aromatic rings. These, in turn, grow mainly through the addition of acetylene. Subsequent growth occurs by coagulation of the large aromatic structures, forming primary soot particles [17]. These primary soot particles will merge, while also picking up additional molecules from the gas along the way, and in the end form more complex irregular shaped aggregates. Despite extensive research into this topic, modeling and predicting soot formation and growth in flames remains challenging [19]. Therefore, experimental studies of the formation and growth of soot are indispensable in adding to our understanding of relevant processes and for improving models of soot formation.

1.3.2. Silica

Concerns over the climate, dwindling energy reserves and the desire for energetic independence are driving the development of renewable energy sources. Biogases can play an important role in a transition from fossil fuels and have seen increasing utilization in recent years; growth in biogas production and use is expected to continue for the foreseeable future [20]. While the exact composition depends on the source, biogas is typically composed of methane and carbon dioxide, with trace amounts of other

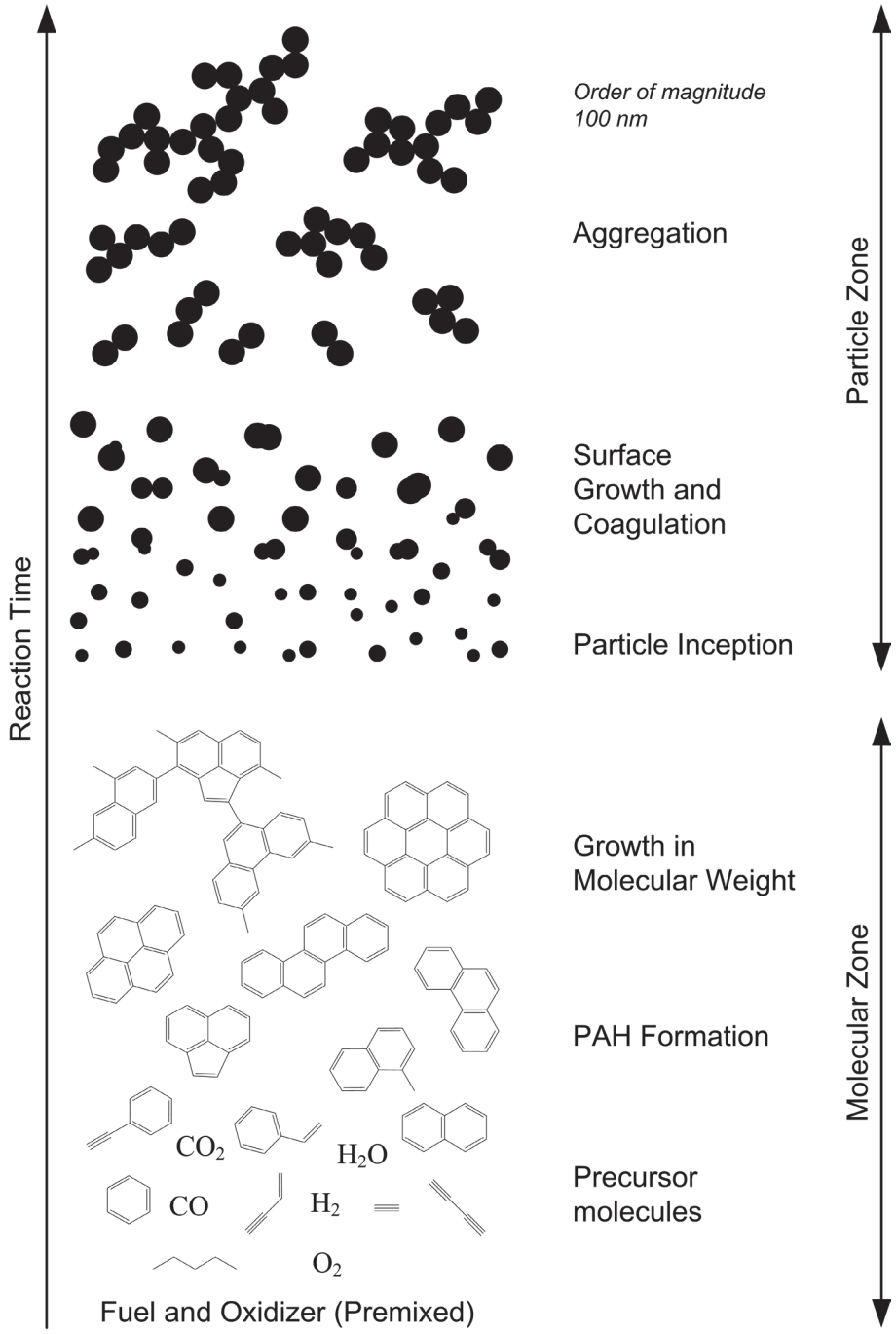

Figure 1.4. *Rough picture of soot formation in a homogeneous hydrocarbon/oxidizer mixture (after Bockhorn [17]).*

constituents, such as sulfide compounds, ammonia, aromatic and halogenated compounds and volatile compounds such as siloxanes [21].

As an impurity in biofuels, siloxanes are of particular interest. Silicon dioxide SiO_2 (a.k.a. silica) generated in the combustion of the siloxanes coalesces into particles that subsequently form aggregates, such as those shown in Figure 1.5, and deposit on internal parts of combustion equipment. Short term effects may be marginal because of the typically low siloxane concentrations (for example, Dewil et al. [22] report values ranging from 4.8 mg/m^3 up to 400 mg/m^3 in biogas from different sites), but it can eventually lead to reduced performance, damage and even equipment failure, which puts limits on acceptable siloxane concentrations [3]. It is important to note that the deleterious effects are not simply a function of the concentration of silica in the flue gases. Whereas the size and structure of silica particles determine their mechanical properties as ceramic powders [23], the structure of silica aggregates are also critical determinants for the impact of deposition in combustion equipment. The deposition of 'fluffy' fractal structures will result in more blocked volume in, for example a heat exchanger, than a denser layer of equal mass; changes in equipment performance have been attributed to this effect [24]. A model describing the growth and properties of these aggregates reliably is therefore essential for formulating realistic limits, which underlines the importance of understanding in detail what happens on the aggregate level.

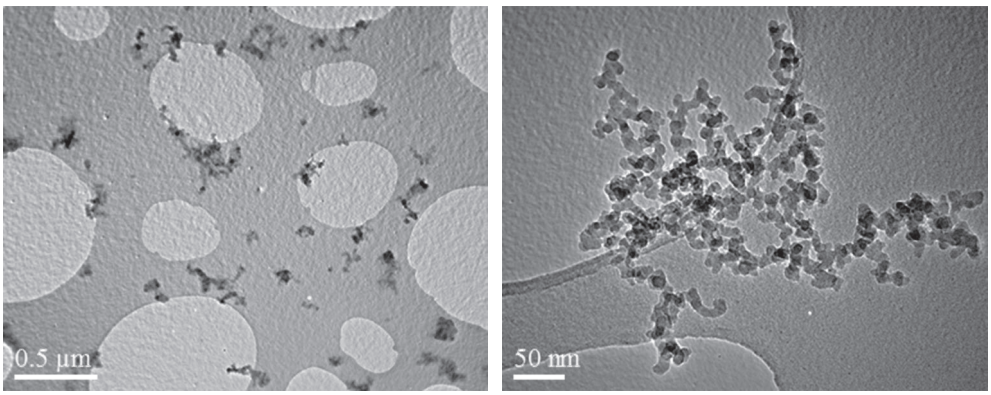

Figure 1.5. *TEM images of typical silica aggregates.*

1.4. Scope and outline of this thesis

This thesis focuses on the laser-based study of combustion-generated nanoparticle growth in premixed flames, in particular of soot and silica. While extensive research has been done

with a focus on aggregate particle growth, additional experimental work is required to add to our understanding of the processes involved and the influence of parameters like temperature, particle volume fraction and fuel/air ratio. An additional interest is that in the effect of hydrogen addition to the fuel. Hydrogen can not only serve to improve the unfavorable combustion characteristics of biogas, but since it does not produce soot and carbon dioxide may also reduce pollutant emission.

0 provides the background on the 1-D premixed burner-stabilized flames that were used in this work to study aggregates. The gas burners and flow control system that were used are detailed here as well. Next, 0 gives an overview of the diagnostic techniques that were used during the work presented in this thesis. The principal techniques used are angle-dependent light scattering (ADLS) to measure particle size, laser light extinction (LLE) and laser-induced incandescence (LII) to measure soot volume fractions, and Raman spectroscopy to measure flame temperatures. This chapter also describes in detail the experimental setups and measurement procedures.

In the subsequent chapters soot and silica aggregate growth are studied. The process of silica particle growth is more straightforward as, in the case of siloxane precursor, all silica is formed very early on. Therefore, it is expected that chemistry can be ignored, and particle growth is the result, solely, of existing material getting bound together into aggregates. The volume fraction of soot on the other hand keeps increasing over time while the process of particle growth through aggregation is already ongoing. Because of its relative simplicity, silica particle formation is studied first. In 0, silica aggregate growth was studied using ADLS in premixed methane/air flames with siloxane admixture, for a range of flame temperatures and siloxane concentrations, and a couple of fuel/air ratios. 0 expands on the previous chapter by looking into the effect of hydrogen addition to the fuel on silica aggregate growth in methane/siloxane/air flames. Next, 0 presents a study of soot in fuel-rich ethylene/air flames, where the techniques described in 0 were used to measure soot particle size as well as volume fraction for a range of flame temperatures and multiple fuel/air ratios. In addition, the measurement results were compared with calculations using two different semi-empirical two-equation models of soot formation. And in 0, the work in 0 was expanded upon by investigating the effect of hydrogen addition on soot aggregate growth in ethylene/air flames.

References

[1] Adachi K, Chung SH, Buseck PR. Shapes of soot aerosol particles and implications for their effects on climate. J Geophys Res Atmos 2010;115:1–9.

[2] Bond TC, Doherty SJ, Fahey DW, Forster PM, Berntsen T, Deangelo BJ, et al. Bounding the role of black carbon in the climate system: A scientific assessment. J Geophys Res Atmos 2013;118:5380–552.

[3] Turkin AA, Dutka M, Vainchtein D, Gersen S, Essen VM van, Visser P, et al. Deposition of SiO2 Nanoparticles in Heat Exchanger During Combustion of Biogas. Appl Energy 2014;113:1141–8.

[4] Zimmer L, Pereira FM, van Oijen JA, de Goey LPH. Investigation of mass and energy coupling between soot particles and gas species in modelling ethylene counterflow diffusion flames. Combust Theory Model 2017;21:358–79.

[5] Kolosnjaj-Tabi J, Just J, Hartman KB, Laoudi Y, Boudjemaa S, Alloyeau D, et al. Anthropogenic Carbon Nanotubes Found in the Airways of Parisian Children. EBioMedicine 2015;2:1697–704.

[6] Niranjan R, Thakur AK. The toxicological mechanisms of environmental soot (black carbon) and carbon black: Focus on Oxidative stress and inflammatory pathways. Front Immunol 2017;8:1–20.

[7] Nichols G, Byard S, Bloxham MJ, Botterill J, Dawson NJ, Dennis A, et al. A review of the terms agglomerate and aggregate with a recommendation for nomenclature used in powder and particle characterization. J Pharm Sci 2002;91:2103–9.

[8] Mandelbrot BB. The Fractal Geometry of Nature. New York: W.H. Freeman and Co.; 1982.

[9] Kruis FE, Kusters KA, Pratsinis SE, Scarlett B. A Simple Model for the Evolution of the Characteristics of Aggregate Particles Undergoing Coagulation and Sintering. Aerosol Sci Technol 1993;19:514–26.

[10] Smirnov BM. Cluster Processes in Gases and Plasmas. Weinheim, Germany: Wiley-VCH Verlag GmbH & Co. KGaA; 2010.

[11] Friedlander SK. Smoke, Dust and Haze: Fundamentals of Aerosol Dynamics. Second. New York: Oxford University Press; 2000.

[12] Fuchs NA. The Mechanics of Aerosols. Oxford: Pergamon Press; 1964.

[13] Seinfeld JH, Pandis SN. Atmospheric Chemistry and Physics: From Air Pollution to Climate Change. 2nd ed. Hoboken, New Jersey: John Wiley & Sons, Inc.; 2006.

[14] Smoluchowski MV. Drei Vortrage uber Diffusion. Brownsche Bewegung und Koagulation von Kolloidteilchen. Z Phys 1916;17:557–85.

[15] Ulrich GD, Riehl JW. Aggregation and Growth of Submicron Oxide Particles in Flames. J Colloid Interface Sci 1982;87:257–65.

[16] Schaap M, Weijers EP, Mooibroek D, Nguyen L, Hoogerbrugge R. Composition and origin of Particulate Matter in the Netherlands. Results from the Dutch Research Programme on Particulate Matter. Bilthoven, The Netherlands: 2010.

[17] Bockhorn H. Soot Formation in Combustion. vol. 59. Berlin, Heidelberg: Springer Berlin Heidelberg; 1994.

[18] Boffetta P, Jourenkova N, Gustavsson P. Cancer risk from occupational and environmental exposure to polycyclic aromatic hydrocarbons. Cancer Causes Control 1997;8:444–72.

[19] Wang H. Formation of nascent soot and other condensed-phase materials in flames. Proc Combust Inst 2011;33:41–67.

[20] Foreest F van. Perspectives for Biogas. Oxford: 2012.

[21] Rasi S. Biogas Composition and Upgrading to Biomethane. University of Jyväskylä, 2009.

[22] Dewil R, Appels L, Baeyens J. Energy use of biogas hampered by the presence of siloxanes. Energy Convers Manag 2006;47:1711–22.

[23] Pratsinis SE. Flame Aerosol Synthesis of Ceramic Powders. Prog Energy Combust Sci 1998;24:197–219.

[24] Gersen S, Visser P, Essen VM van, Dutka M, Vainchtein D, Hosson JTM de, et al. Effects of Silica Deposition on the Performance of Domestic Equipment. Proc. Eur. Combust. Meet., 2013.